Host-Guest Interactions in C_2H_2/CO_2 Discriminative Covalent Organic Framework Probed by Solid-State NMR

Weiming Jiang[1], Ping Wang[2], Ken-ichi Otake[2], Susumu Kitagawa[2], Yasuto Noda[1]*, Kazuyuki Takeda[1]*, Kiyonori Takegoshi[1]

[1]Division of Chemistry, Graduate School of Science, Kyoto University, 606-8502 Kyoto, Japan

[2]Institute for Integrated Cell-Material Sciences, Kyoto University Institute for Advanced Study, Kyoto University, 606-8501 Kyoto, Japan

ABSTRACT: Covalent organic frameworks (COF) are promising porous materials for energy-efficient gas separation. However, understanding of the interaction between the host framework and the guest gas molecules, which is crucial for the development of the COF adsorbents, remains insufficient. Here, we look into the host-guest interactions between C_2H_2/CO_2 molecules and a propyl sodium sulfonate group functionalized COF. Gas sorption studies indicate that the synthesized COF, termed Py-Na COF, exhibits C_2H_2/CO_2 discriminative adsorption at ambient temperature. The underlying discriminative mechanism is studied by in situ ^{23}Na solid-state NMR combined with molecular dynamics (MD) and density functional theory (DFT) calculations. The interactions between the C_2H_2/CO_2 molecules and the host sodium ion play an essential role in C_2H_2/CO_2 discrimination in Py-Na COF.

Covalent organic frameworks (COFs) are an emerging class of porous crystalline materials with high designability, functionality, and robustness[1-5], and have been utilized to separate gases such as carbon dioxide (CO_2)/nitrogen (N_2)[6-7], CO_2/methane (CH_4)[8-9], acetylene (C_2H_2)/ethylene (C_2H_4)[10]. Appropriate interactions between the adsorbents and the host molecules are the keys to enhancing the performance of separation. So far, various strategies of modifying COFs, including pore dimension/topology design[11-13] and pore surface decoration,[6,14-17] have been reported. To make the COFs next-generation adsorbent materials alleviating energy consumption of gas storage and separation, it is desirable to realize efficient discriminative adsorption of C_2H_2 over CO_2.[18] It is, however, challenging, since their dimensions ($3.32 \times 3.34 \times 5.7$ Å^3 for C_2H_2, $3.18 \times 3.33 \times 5.36$ Å^3 for CO_2) and physical properties (boiling points of 189.3 and 194.7 K for C_2H_2 and CO_2, respectively) are almost identical,[19] and in addition, they are both apolar.[20]

Accordingly, any physisorption-based separation strategy needs to exploit the difference in the quadrupole moments of the C_2H_2 and CO_2 molecules. Since the quadrupole moment of C_2H_2 is of opposite sign and has a greater absolute value compared to that of CO_2, introducing appropriate electrostatic interactions into the porous framework potentially leads to efficient discrimination of the C_2H_2 and CO_2 molecules. So far, integrating hydrogen sulfonic groups has proven to be effective for improving the uptake of CO_2 by metal organic frameworks.[21-22] However, the hydrogen sulfonic groups cooperated in the porous frameworks also attract C_2H_2, offering no help to separate C_2H_2/CO_2.[23] By replacing the proton of the sulfonate group in the porous materials with sodium or silver ions, C_2H_2/C_2H_4 selectivity has successfully been enhanced, owing to the additional cation-π electrostatic interaction.[24-25]

Here, we present a COF functionalized with the sodium sulfonic group which exhibits discriminative adsorption towards C_2H_2 over CO_2 at ambient temperature. The COF, referred to as Py-Na COF, is composed of 4,4′,4″,4‴-(pyrene-1,3,6,8-tetrayl) tetraaniline (PyTTA) and 2,5-di(oxypropane-1-sodium sulfonate) terephthalaldehyde (DSTA) unit with imine linkage (Fig. 1(a)). In the following, we show molecular dynamics (MD) calculations of Py-Na COF loaded with C_2H_2 or CO_2 revealing the interactive sites and configurations. To evaluate the effects of binding of the C_2H_2 and CO_2 molecules with the Py-Na COF, we then calculate ^{23}Na NMR parameters of the sodium sulfonate group by density functional theory (DFT) and experimentally examine them by in-situ gas-loaded ^{23}Na high-resolution solid-state NMR (SSNMR) spectroscopy utilizing a homebuilt hermetic rotor and a gas loading system (Fig. S1).

We synthesized Py-Na COF using DSTA and PyTTA via hydrothermal condensation in *n*-butanol solvent with 6 M acetic acid as catalyst (see Section 1.2 of Supporting Information for details). The structure of Py-Na COF was characterized by Fourier transform infrared (FT-IR) spectroscopy, powder X-ray diffraction (PXRD), scanning electron microscopy (SEM), and SSNMR. The formation of the imine linkage was confirmed by the appearance of the band of C=N stretching vibration at 1613 cm^{-1} in the FT-IR spectrum (Fig S3) and the imine peak at 152 ppm in the ^{13}C cross polarization-magic angle spinning (CP-MAS) spectrum (Fig S4). The S=O peak at 1040 cm^{-1} in the FT-IR spectrum and three distinct alkyl carbon peaks between 20-70 ppm in the ^{13}C spectrum indicate successful anchoring of the propyl sulfonate side chains. The SEM image of Py-Na COF (Fig. S5) revealed the stacked configuration of rod-shaped crystallites. Thermogravimetric analysis indicated that Py-Na COF possesses high thermal stability up to 250 °C (Fig. S6). The crystal structure was found to be intact without significant change in the PXRD pattern for one year (Fig. S7).

The crystal structure of Py-Na COF in space group *C*2/*m* was modeled with the unit cell parameter optimized by Pawley refinement of the experimental PXRD pattern (Fig. 1(b)). The simulated PXRD pattern of the AA stacking model with the optimized unit cell matched the experimental results (Fig. S8, S9). The unit cell parameters (a = 33.25 Å, b = 34.40 Å, c = 3.95 Å and $\alpha = \gamma =$

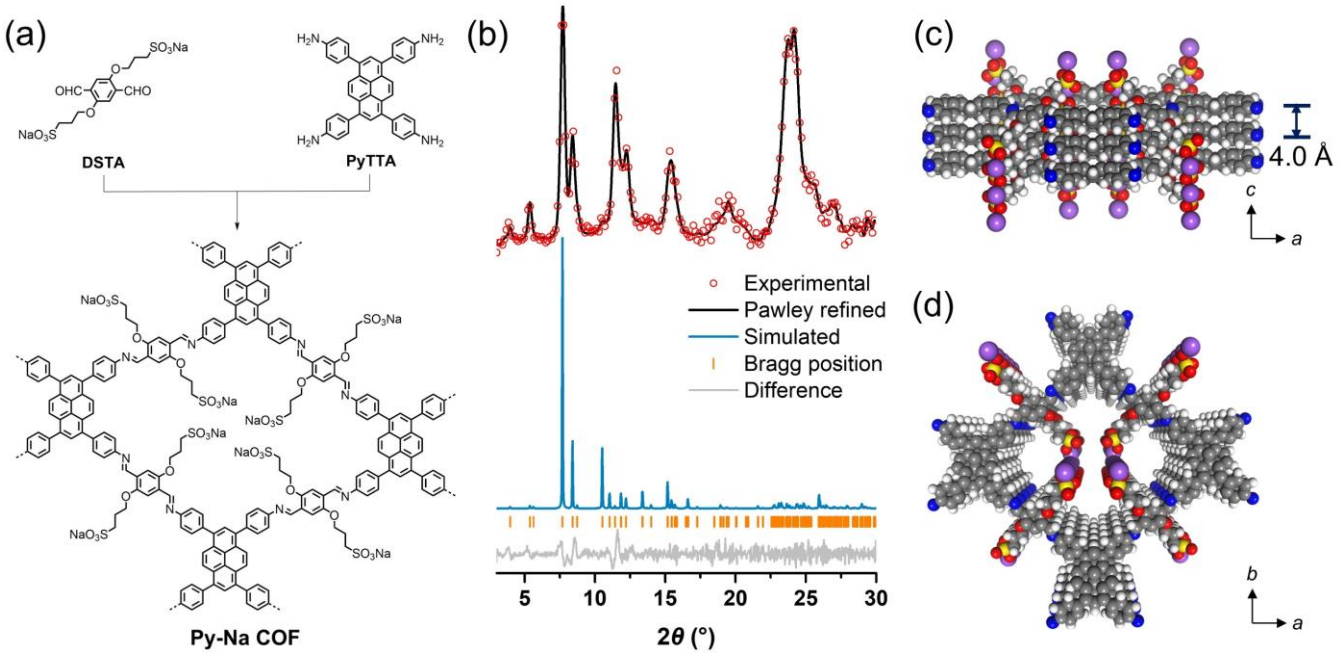

Figure 1. (a) Schematic representation of the synthesis of Py-Na COF. (b) Experimental (red circle), Pawley refined (black), simulated eclipsed AA stacking (blue) of powder X-ray diffraction patterns for Py-Na COF. The bottom gray line is the difference between the experimental and the refined patterns. (c) Side and (d) Top view of the reconstructed crystal structure of Py-Na COF. (gray: C, white: H, blue: N, red: O, yellow: S, purple: Na).

90°, β = 80°) were obtained with reliability factors R_p and R_{wp} of 6.43 % and 8.56 %. The discrepancy between 2θ range 10°-13° of the simulated pattern and the experimental PXRD pattern is ascribed to the interlayer shift of Py-Na COF induced by the side chains, which is similar to that induced by the solvation effect reported for a derivative of Py-Na COF with the same skeleton.[26] From the reconstructed eclipsed AA stacking crystal structure of Py-Na COF shown in Fig. 1(c)(d), the size of the pore aperture was estimated to be ca. 0.5 nm.

The porosity of Py-Na COF was characterized by N_2 adsorption isotherm at 77 K. The N_2 uptake was lower than 20 cm^3 at pressures P/P_0 < 0.8, and rapidly increased with the pressure for P/P_0 higher than 0.9 up to near the saturation level (Fig. S10). We ascribe the low uptake at the low pressure to the inefficient diffusion of the N_2 molecules in ultramicropores with a pore diameter less than 0.7 nm and the sharp rise to the condensation of the N_2 molecules in inter-particle voids.[27] Thus, the aperture size estimated from the isotherm and that from the reconstructed structure are consistent with each other.

Figure 2 shows C_2H_2 and CO_2 adsorption isotherms measured at 195 K, 273 K, and 298 K. At 195 K, Py-Na COF exhibited similar C_2H_2 and CO_2 adsorption isotherms, so that the capacities of C_2H_2 and CO_2 are nearly the same. At 273 K, the greater capacity of C_2H_2 over CO_2 for Py-Na COF at the whole pressure range suggested the host-guest interaction affected adsorption behavior at near ambient temperature.

When the temperature increased to 298 K, Py-Na COF showed the C_2H_2 capacity of 38 cm^3g^{-1} at 1 bar, which is approximately double that for CO_2 (20 cm^3g^{-1}) under the same condition. The selectivity, calculated at room temperature by the equimolar C_2H_2/CO_2 adsorption of Py-Na COF using the ideal adsorbed solution theory (IAST), was over 7 in the 0-100 kPa range (Fig. S13) (see Section 3 of Supporting Information for details).

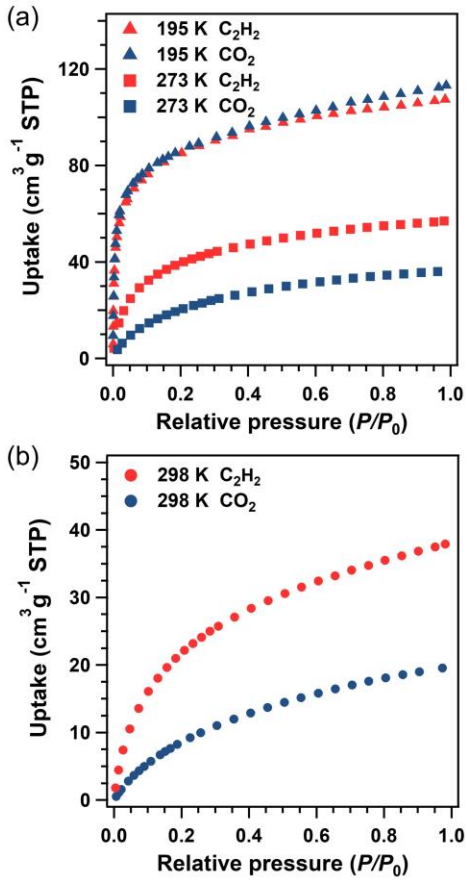

Figure 2. C_2H_2 and CO_2 adsorption for Py-Na COF at (a) 195 K and 273 K (b) 298 K.

To identify the interaction site, evaluate the effect of the guest on the host, and thereby shed light on the origin of the C_2H_2/CO_2 discriminative adsorption behavior of Py-Na COF, we carried out MD and DFT calculations. (see Section 4 of Supporting Information for details).

We calculated the potential fields for the C_2H_2 and CO_2 molecules inside the pore of Py-Na COF by the grand canonical Monte Carlo (GCMC) method using the optimized structures of Py-Na COF supercell and the C_2H_2/CO_2 molecules.[28] The calculated potential fields (Fig. S14) show that, for C_2H_2, the preferential adsorption region is relatively close to the sodium sulfonate groups with an interactive strength of up to −40 kJ mol^{-1}, whereas the preferential regions for CO_2 are more dispersed with the weaker interaction (~ −35 kJ mol^{-1}) compared to the former.

Figure 3(a) shows the configuration of one C_2H_2 molecule adsorbed in Py-Na COF that gave the lowest energy calculated by the GCMC method. The binding of the C_2H_2 molecule to Py-Na COF is such that one of the carbon atoms of the C_2H_2 molecule tends to approach the sodium ion. Conversely, the CO_2 molecule was found to settle in a different site relatively distant from the sodium ion, as shown in Fig. 3(b).

Simulated isotherms of C_2H_2/CO_2 for the Py-Na COF supercell by the GCMC method resulted in similar uptakes of C_2H_2 and CO_2 at 195 K and approximately double uptake of C_2H_2 over CO_2 at 1 bar, 298 K (Fig. S15, S16), showing the same trend as the experimental adsorption results except for overestimated amounts. In addition, the calculated isosteric heats (Q_{st}) for C_2H_2 and CO_2 adsorption (−47.3 kJ·mol^{-1}for C_2H_2 and −32.5 kJ·mol^{-1} for CO_2) were consistent with the Q_{st} values obtained from the experimental isotherms for Py-Na COF at 273 K and 298 K (−49.0 kJ·mol^{-1} C_2H_2 and −41.2 kJ·mol^{-1} for CO_2). The greater absolute value of Q_{st} for C_2H_2 adsorption suggests that Py-Na COF has the higher C_2H_2 affinity.

To reflect more realistic situations, we took the flexibility and disorder of the side chains into account by annealing the supercell structure of Py-Na COF at 298 K. As a consequence, the side chains twisted and the head of the sulfonate sodium group randomly pointed to all directions (Fig. 3(c)). The adsorption isotherm simulated for this annealed supercell still displayed the same discriminative adsorption behavior of C_2H_2 over CO_2 with reduced uptakes compared to the ideal cell (Fig. S15). This result suggests that the disorder reduces pore space and thereby restrains adsorption. Nevertheless, the discriminative ability is not significantly affected by the complexity of the structure, since the interactive sites can still discriminate the guest molecules in a synergetic and complex way as long as they are accessible.

DFT calculations of the NMR parameters based on this optimized supercell structure are hindered by the high computational cost. Accordingly, we made a simplified model composed of a single fragment of Py-Na COF and the guest molecules in a cell (40 × 40 × 20 Å^3), and then obtained the several lowest energy configurations of the fragment that interacted with the guest molecules by the GCMC method (Fig. S17, S18). We found that for all of these lowest energy configurations, the C_2H_2 or CO_2 molecule was bound to the sodium sulfonate group of the fragment. The calculated spatial location of C_2H_2 in the cell displayed more concentrated distribution around the sulfonate group compared to CO_2 (Fig. S19). Figure. S20 shows electrostatic potential maps obtained from the optimized structure and configurations.

To evaluate the effect of the guest binding to the local environment of the sodium ion, we numerically calculated the chemical shielding and the quadrupolar parameters of the ^{23}Na nucleus by the CASTEP module (Table. S1) and analyzed the isotropic terms for further comparison with SSNMR experiments. We found that when the C_2H_2 molecule was bound to the Na^+ site, the average value of isotropic chemical shielding (σ_{iso}) of Na^+ was lower by approximately 20 ppm than that obtained with the guest-free condition. Conversely, the CO_2 molecule has a similar but much smaller effect on the ^{23}Na shielding than the C_2H_2 molecule does. This result suggests that both C_2H_2 and CO_2 interact with Na^+, while the effect of the former on the sodium ion is greater.

To verify if the interactive site, configuration, and the effect of binding obtained by the MD and DFT calculations are reasonable, we carried out gas-loaded in-situ high-resolution SSNMR measurements. A hermetic rotor packed with Py-Na COF was put into the gas loading setup connected to a vacuum pump and gas cylinders (Fig. S1). The sample was evacuated under heat, loaded with gases to 2 bar at room temperature, and then subjected to SSNMR line, proving successful accommodation of C_2H_2 in Py-Na COF (Fig. S21). The airtightness of the hermetic rotor was verified by monitoring the peak intensity of C_2H_2 using an arrayed ^{1}H MAS NMR experiment over hours (Fig. S22).

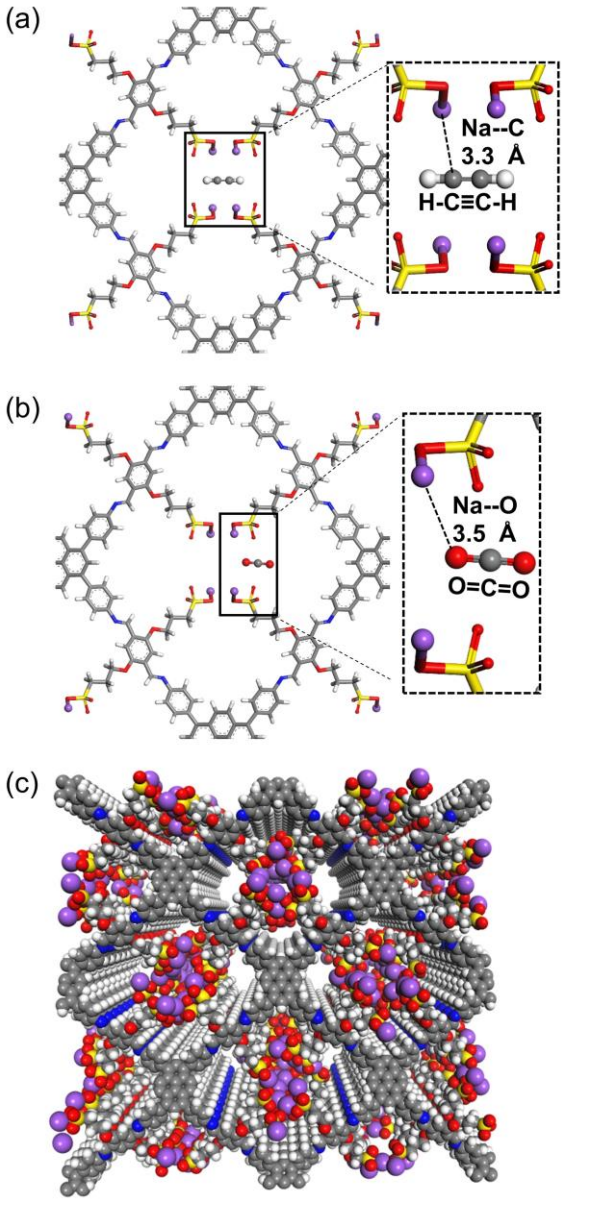

Figure 3. Simulated binding configuration of (a) C_2H_2 (b) CO_2 in Py-Na COF. (Na--C: 3.3 Å, Na--O: 3.5 Å) (c) Annealed supercell structure of Py-Na COF at 298 K.

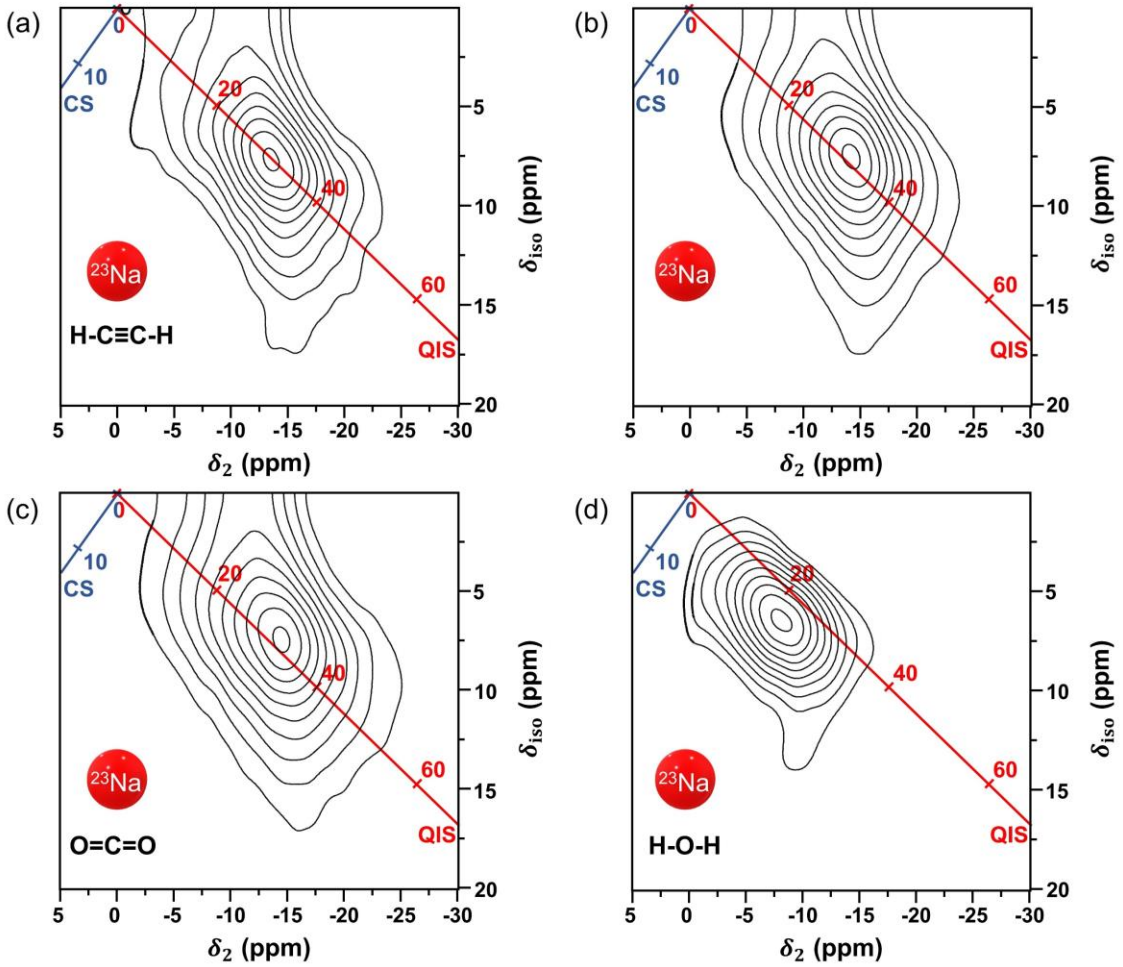

Figure 4. 2D ^{23}Na split-t_1 3QMAS spectra of Py-Na COF in (a) C_2H_2 (b) vacuum (c) CO_2 (d) air. CS (blue) and QIS (red) are the chemical shift and quadrupolar induced shift axes (unit: ppm).

In ^{13}C CP-MAS NMR spectra of Py-Na COF under air, CO_2, and C_2H_2 conditions (Fig. S23), no discernible change in the peak components or positions for the carbon framework was found, which means all the guest molecules have no obvious interaction with the carbon skeleton. Since CP-MAS does not give rise to signals from highly mobile species like free gases, the ^{13}C signal of C_2H_2 at 72 ppm in the ^{13}C CP-MAS spectrum of the C_2H_2 loaded sample (Fig. S21) indicates that the motion of C_2H_2 is restricted. It follows that there exists an interaction between C_2H_2 and the host at some binding sites other than the carbon skeleton.

In ^{23}Na MAS NMR of Py-Na COF, we noticed appreciable changes in the position of the single broad featureless peak under different conditions (Fig. S24). ^{23}Na is a spin-3/2 quadrupolar nucleus, and its resonance is perturbed by both the chemical shielding and the quadrupolar shift induced by the electric field gradient at the nucleus. Thus, the peak position, i.e., the center of mass $\overline{\delta_2}$ of the resonance line, reflects the effects of both the averaged isotropic contributions $\overline{\delta^{CS}}$ of the chemical shift and that $\overline{\delta^{Q}}$ of the quadrupolar interaction.

To extract the contribution of the chemical *shift* for comparison with the chemical *shielding* obtained by the DFT calculation, we then carried out two-dimensional (2D) ^{23}Na split-t_1 3QMAS experiments (Fig. 4),[29] in which the contributions of the chemical shift $\delta^{CS}$and the quadrupolar interaction δ^{Q} can be obtained separately and the anisotropy is removed along the indirect dimension (δ_{iso}), so that the broadening in Fig. 4 along δ_{iso} indicates distributions of δ^{CS} and δ^{Q}. The blue and red lines in Fig. 4 are the chemical shift (CS) and the quadrupolar induced shift (QIS) axes plotted according to the Massiot convention,[30] along which the effect of the distribution of δ^{CS} and δ^{Q} appears separately. The position of the ^{23}Na peak of the C_2H_2-loaded sample shifted in both the δ_{iso} and δ_2 axes compared to the evacuated sample (Fig. 4(a)(b)). Contrastively, no appreciable shift of ^{23}Na resonance was observed in both axes for the CO_2-loaded sample (Fig. 4(c)).

The isotropic contributions $\overline{\delta^{CS}}$ and $\overline{\delta^{Q}}$ were obtained from the peak position $\overline{\delta_{iso}}$ and $\overline{\delta_2}$, and summarized in Table S2 (see Section 5.1 of Supporting Information for details). The isotropic chemical shift δ_{iso}^{CS} and the shielding parameter σ_{iso} are related by $\delta_{iso}^{CS} = \overline{\delta^{CS}} = \sigma_{ref} - \sigma_{iso}$, where σ_{ref} is the shielding parameter of the reference compound. The experimentally obtained downfield shift of δ_{iso}^{CS} of the ^{23}Na resonance induced by the binding of the C_2H_2 molecule is consistent with the decrease in σ_{iso} obtained by the DFT numerical calculation, and therefore supports the structure and configuration of C_2H_2-loaded Py-Na COF that led to the lowest calculated energy as shown in Fig. 3, S17, S18.

All the 2D spectra did not exhibit discrete peaks of distinct sodium sites but a broad resonance line in the δ_{iso} axis. The broadening in the δ_{iso} axis arose solely from the distribution of δ^{CS} and

δ^{Q}, where the distribution of δ^{Q} along the QIS axis dominantly contributed to the broadening. Such distribution, which is typical for glassy materials, indicates the presence of disorder of the sodium ions in Py-Na COF.[31]

For the air-exposed Py-Na COF sample, the ^{23}Na resonance measured by 3QMAS also shifted (Fig. 4(d)). Presumably, the H_2O molecule in the air coordinates to Na^+ to form a hydrate ion. The changes in the chemical shielding and the quadrupolar parameters of ^{23}Na are the consequences of the changes in the electronic environment around Na^+ introduced by the guest molecules. Thus, we confirm that the sodium ion is indeed the interactive site for these guest molecules. The larger ^{23}Na chemical shift for the C_2H_2-loaded sample than that for the CO_2-loaded sample suggests the stronger interaction between C_2H_2 and Na^+. We also found the loading of the gases did not significantly change the quadrupolar parameters in both the calculations and the experiments (Table S1). This indicates the binding of the gas molecule to Na^+ is not as strong as the coordination bonds.

It should be noted, however, that the shift of δ_{iso}^{CS} was an order of magnitude smaller than that obtained by the calculation. The dominant factor causing the discrepancy is the difference in the quantity between the real adsorption process and the DFT calculation. The saturation uptake of C_2H_2 and CO_2 for Py-Na COF at 298 K is 0.6 C_2H_2 molecule per Na^+ and 0.3 CO_2 molecule per Na^+, which are both less than that in the 1:1 model used for the DFT numerical calculation. In addition, the significantly smaller experimental shift implies that the individual interactive site dynamically undergoes the adsorption and desorption processes, so that the shift appears to be the averaged one between the guest-bound and the vacuum conditions.

The electrostatic potential map obtained from the optimized structure and configuration (Fig. S20(a)) indicates that the negatively charged region of the C_2H_2 molecule around the triple bond is attracted to the sodium cation. In the case of CO_2, it is one of the edges of the molecule that is negatively charged and thereby is attracted to the sodium cation (Fig. S20(b)). It follows that the molecule can also bind to the sodium sulfonate group, but only with a relatively longer distance compared to the case of C_2H_2. These configurations also explain the reason why the hydrogen sulfonic group in the porous framework failed and the sodium sulfonate group succeeded in discriminating C_2H_2 and CO_2.[21] The additional, energetically favorable quadrupolar cation-π interaction would develop between the alkali metal ions and the gas molecules that include π electrons. For Py-Na COF, the cation-π interaction between the sodium ion and the C_2H_2 molecules leads to both the shifts of the ^{23}Na NMR peak and the discriminative adsorption of C_2H_2 over CO_2.

In summary, Py-Na COF synthesized in this work showed discriminative adsorption of C_2H_2 over CO_2 at room temperature. The in-situ ^{23}Na 3QMAS NMR measurements and the calculations suggested that the sodium sulfonate group is the interactive site for both C_2H_2 and CO_2, with the greater affinity to the former due to the additional quadrupolar cation-π interaction. This work not only enriches the family of COF-based sorbents for challenging gas separation, but also paves the way for mechanistic studies of gas discrimination utilizing the SSNMR techniques.

ASSOCIATED CONTENT

Supporting Information

Materials and instruments, characterizations, Q_{st} and IAST selectivity calculation, MD and DFT calculation details, solid-state NMR spectra, unit cell parameters are included in the supporting information.

Notes

The authors declare no competing financial interests.

AUTHOR INFORMATION

Corresponding Author

Noda Yasuto – Division of Chemistry, Graduate School of Science, Kyoto University, 606-8502 Kyoto, Japan; ORCID: 0000-0003-4971-4023
Email: noda@kuchem.kyoto-u.ac.jp
Takeda Kazuyuki – Division of Chemistry, Graduate School of Science, Kyoto University, 606-8502 Kyoto, Japan; ORCID: 0000-0002-6743-0932
Email: takezo@kuchem.kyoto-u.ac.jp

ACKNOWLEDGMENT

This work was supported by JSPS Grant-in-Aid for Scientific Research on Innovation Areas “Mixed anion” (grant number 16H06440). Computation time was provided by the Super Computer System, Institute for Chemical Research, Kyoto University. We would thank Prof. Satoshi Horike and Ms. Nanae Shimanaka of iCeMS, Kyoto University for the SEM and TGA measurements.

REFERENCES

(1) Liu, R.; Tan, K. T.; Gong, Y.; Chen, Y.; Li, Z.; Xie, S.; He, T.; Lu, Z.; Yang, H.; Jiang, D., Covalent organic frameworks: an ideal platform for designing ordered materials and advanced applications. *Chem. Soc. Rev.* **2021**, *50* (1), 120-242.
(2) Tao, S.; Zhai, L.; Dinga Wonanke, A. D.; Addicoat, M. A.; Jiang, Q.; Jiang, D., Confining H_3PO_4 network in covalent organic frameworks enables proton super flow. *Nat. Commun.* **2020,** *11* (1), 1981.
(3) Gropp, C.; Ma, T.; Hanikel, N.; Yaghi, O. M., Design of higher valency in covalent organic frameworks. *Science* **2020,** *370* (6515), eabd6406.
(4) Zhao, C.; Lyu, H.; Ji, Z.; Zhu, C.; Yaghi, O. M., Ester-Linked Crystalline Covalent Organic Frameworks. *J. Am. Chem. Soc.* **2020,** *142* (34), 14450-14454.
(5) An, S.; Xu, Q.; Ni, Z.; Hu, J.; Peng, C.; Zhai, L.; Guo, Y.; Liu, H., Construction of Covalent Organic Frameworks with Crown Ether Struts. *Angew. Chem. Int. Ed.* **2021,** *60* (18), 9959-9963.
(6) Huang, N.; Krishna, R.; Jiang, D., Tailor-Made Pore Surface Engineering in Covalent Organic Frameworks: Systematic Functionalization for Performance Screening. *J. Am. Chem. Soc.* **2015,** *137* (22), 7079-7082.
(7) Ge, R.; Hao, D.; Shi, Q.; Dong, B.; Leng, W.; Wang, C.; Gao, Y., Target Synthesis of an Azo (N═N) Based Covalent Organic Framework with High CO_2-over-N_2 Selectivity and Benign Gas Storage Capability. *J. Chem. Eng. Data* **2016,** *61* (5), 1904-1909.
(8) Li, Z.; Feng, X.; Zou, Y.; Zhang, Y.; Xia, H.; Liu, X.; Mu, Y., A 2D azine-linked covalent organic framework for gas storage applications. *Chem. Commun.* **2014,** *50* (89), 13825-13828.
(9) Shan, M.; Seoane, B.; Rozhko, E.; Dikhtiarenko, A.; Clet, G.; Kapteijn, F.; Gascon, J., Azine-Linked Covalent Organic Framework (COF)-Based Mixed-Matrix Membranes for CO_2/CH_4 Separation. *Chem. Eur. J.* **2016,** *22* (41), 14467-14470.
(10) Jiang, L.; Tian, Y.; Sun, T.; Zhu, Y.; Ren, H.; Zou, X.; Ma, Y.; Meihaus, K. R.; Long, J. R.; Zhu, G., A Crystalline Polyimide Porous Organic Framework for Selective Adsorption of Acetylene over Ethylene. *J. Am. Chem. Soc.* **2018,** *140* (46), 15724-15730.
(11) Wang, P.; Chen, X.; Jiang, Q.; Addicoat, M.; Huang, N.; Dalapati, S.; Heine, T.; Huo, F.; Jiang, D., High-Precision Size Recognition and Separation in Synthetic 1D Nanochannels. *Angew. Chem. Int. Ed.* **2019,** *58* (44), 15922-15927.
(12) Fan, H.; Peng, M.; Strauss, I.; Mundstock, A.; Meng, H.; Caro, J., MOF-in-COF molecular sieving membrane for selective hydrogen separation. *Nat. Commun.* **2021,** *12* (1), 38.
(13) Mohammed, A. K.; Usgaonkar, S.; Kanheerampockil, F.; Karak, S.; Halder, A.; Tharkar, M.; Addicoat, M.; Ajithkumar, T. G.; Banerjee, R., Connecting Microscopic Structures, Mesoscale Assemblies, and Macroscopic Architectures in 3D-Printed Hierarchical Porous Covalent Organic Framework Foams. *J. Am. Chem. Soc.* **2020**, *142* (18), 8252-8261.

(14) Gao, C.; Li, J.; Yin, S.; Lin, G.; Ma, T.; Meng, Y.; Sun, J.; Wang, C., Isostructural Three-Dimensional Covalent Organic Frameworks. *Angew. Chem. Int. Ed.* **2019,** *58* (29), 9770-9775.
(15) Huang, N.; Chen, X.; Krishna, R.; Jiang, D., Two-Dimensional Covalent Organic Frameworks for Carbon Dioxide Capture through Channel-Wall Functionalization. *Angew. Chem. Int. Ed.* **2015,** *54* (10), 2986-2990.
(16) Lin, R.-B.; Xiang, S.; Zhou, W.; Chen, B., Microporous Metal-Organic Framework Materials for Gas Separation. *Chem* **2020,** *6* (2), 337-363.
(17) Lohse, M. S.; Bein, T., Covalent Organic Frameworks: Structures, Synthesis, and Applications. *Adv. Funct. Mater.* **2018,** *28* (33), 1705553.
(18) Chen, L.; Gong, C.; Wang, X.; Dai, F.; Huang, M.; Wu, X.; Lu, C.-Z.; Peng, Y., Substoichiometric 3D Covalent Organic Frameworks Based on Hexagonal Linkers. *J. Am. Chem. Soc.* **2021,** *143* (27), 10243-10249.
(19) Reid, C. R.; Thomas, K. M., Adsorption Kinetics and Size Exclusion Properties of Probe Molecules for the Selective Porosity in a Carbon Molecular Sieve Used for Air Separation. *J. Phys. Chem. B* **2001,** *105* (43), 10619-10629.
(20) Matsuda, R.; Kitaura, R.; Kitagawa, S.; Kubota, Y.; Belosludov, R. V.; Kobayashi, T. C.; Sakamoto, H.; Chiba, T.; Takata, M.; Kawazoe, Y.; Mita, Y., Highly controlled acetylene accommodation in a metal-organic microporous material. *Nature* **2005,** *436* (7048), 238-41.
(21) Lu, W.; Yuan, D.; Sculley, J.; Zhao, D.; Krishna, R.; Zhou, H.-C., Sulfonate-Grafted Porous Polymer Networks for Preferential CO_2 Adsorption at Low Pressure. *J. Am. Chem. Soc.* **2011,** *133* (45), 18126-18129.
(22) Hu, Z.; Zhang, K.; Zhang, M.; Guo, Z.; Jiang, J.; Zhao, D., A combinatorial approach towards water-stable metal-organic frameworks for highly efficient carbon dioxide separation. *Chem. Sus. Chem.* **2014,** *7* (10), 2791-5.
(23) Colombo, V.; Montoro, C.; Maspero, A.; Palmisano, G.; Masciocchi, N.; Galli, S.; Barea, E.; Navarro, J. A., Tuning the adsorption properties of isoreticular pyrazolate-based metal-organic frameworks through ligand modification. *J. Am. Chem. Soc.* **2012,** *134* (30), 12830-43.
(24) Tao, Y.; Krishna, R.; Yang, L. X.; Fan, Y. L.; Wang, L.; Gao, Z.; Xiong, J. B.; Sun, L. J.; Luo, F., Enhancing C_2H_2/C_2H_4 separation by incorporating low-content sodium in covalent organic frameworks. *Inorg. Chem. Front.* **2019,** *6* (10), 2921-2926.
(25) Li, B.; Zhang, Y.; Krishna, R.; Yao, K.; Han, Y.; Wu, Z.; Ma, D.; Shi, Z.; Pham, T.; Space, B.; Liu, J.; Thallapally, P. K.; Liu, J.; Chrzanowski, M.; Ma, S., Introduction of π-Complexation into Porous Aromatic Framework for Highly Selective Adsorption of Ethylene over Ethane. *J. Am. Chem. Soc.* **2014,** *136* (24), 8654-8660.
(26) Kang, C.; Zhang, Z.; Wee, V.; Usadi, A. K.; Calabro, D. C.; Baugh, L. S.; Wang, S.; Wang, Y.; Zhao, D., Interlayer Shifting in Two-Dimensional Covalent Organic Frameworks. *J. Am. Chem. Soc.* **2020,** *142* (30), 12995-13002.
(27) Thommes, M., Physical Adsorption Characterization of Nanoporous Materials. *Chem. Ing. Tech.* **2010,** *82* (7), 1059-1073.
(28) Pang, J.; Jiang, F.; Wu, M.; Liu, C.; Su, K.; Lu, W.; Yuan, D.; Hong, M., A porous metal-organic framework with ultrahigh acetylene uptake capacity under ambient conditions. *Nat. Commun.* **2015,** *6* (1), 7575.
(29) Brown, S. P.; Wimperis, S., Two-Dimensional Multiple-Quantum MAS NMR of Quadrupolar Nuclei: A Comparison of Methods. *J. Magn. Reson.* **1997,** *128* (1), 42-61.
(30) Massiot, D.; Touzo, B.; Trumeau, D.; Coutures, J. P.; Virlet, J.; Florian, P.; Grandinetti, P. J., Two-dimensional magic-angle spinning isotropic reconstruction sequences for quadrupolar nuclei. *Solid State Nucl. Magn. Reson.* **1996,** *6* (1), 73-83.
(31) Angeli, F.; Delaye, J. M.; Charpentier, T.; Petit, J. C.; Ghaleb, D.; Faucon, P., Influence of glass chemical composition on the Na–O bond distance: a ^{23}Na 3Q-MAS NMR and molecular dynamics study. *J. Non-Cryst. Solids* **2000,** *276* (1), 132-144.